

Solar Drying of Sludge from a Steel-Wire-Drawing Industry

Gonçalves Lindomar Matias, Mendoza-Martinez Clara, Rocha Elém Patrícia Alves,
de Paula Eduardo Coutinho, Cardoso Marcelo

This is a Publisher's version version of a publication
published by MDPI
in Energies

DOI: 10.3390/en16176314

Copyright of the original publication:

© 2023 by the authors.


Please cite the publication as follows:

Matias Gonçalves, L.; Mendoza-Martinez, C.; Alves Rocha, E.P.; Coutinho de Paula, E.;
Cardoso, M. Solar Drying of Sludge from a Steel-Wire-Drawing Industry. Energies 2023, 16,
6314. <https://doi.org/10.3390/en16176314>

**This is a parallel published version of an original publication.
This version can differ from the original published article.**

Article

Solar Drying of Sludge from a Steel-Wire-Drawing Industry

Lindomar Matias Gonçalves ^{1,2}, Clara Mendoza-Martinez ^{3,*} , Elém Patrícia Alves Rocha ⁴,
Eduardo Coutinho de Paula ² and Marcelo Cardoso ²

¹ Institute of Pure and Applied Sciences, Federal University of Itajubá, Rua Irmã Ivone Drumond, 200-Indu Trial District II, Itabira 35903-087, Brazil

² Department of Environmental Engineering, Federal University of Minas Gerais, Av. Antônio Carlos 6627, Belo Horizonte 31270-901, Brazil

³ School of Energy Systems, LUT University, Yliopistonkatu 34, FI-53850 Lappeenranta, Finland

⁴ Department of Materials Engineering, Federal University of the Jequitinhonha and Mucuri Valleys, Campus Janaúba, Av. Um 4050, Janaúba 39447-901, Brazil

* Correspondence: clara.mendoza.martinez@gmail.com

Abstract: Steel is a crucial industrial product with applications in various sectors, such as construction, engineering, and industry. However, the steel industry generates significant waste, contributing to greenhouse gas emissions and environmental challenges. To address this issue, incorporating solid waste, especially sludge with high moisture content, into the steel industry's operations is essential. This study aimed to construct and test an active indirect solar dryer for reducing the moisture content of sludge from a steel drawing industry. By employing principles of the circular economy and the environmental, social, and governance concept, the drying process showed promising results, achieving approximately 42% moisture reduction. This study involved collection and characterization of industrial sludge, design and assembly of a hybrid active indirect solar dryer, fluid dynamic analysis of the behavior of the air inside the device through CFD Ansys software 2012, tests with a thermographic camera to validate the simulation, and optimization of the sludge drying by calculating the thermal efficiency and drying efficiency of the equipment. The adoption of such drying processes can lead to substantial cost reductions in the transportation, handling, and landfilling of steel-drawing sludge, promoting innovation and aiding global steel industries in achieving their solid waste disposal targets.

Keywords: circular economy; hybrid indirect solar dryer; steel industry; CFD; industrial waste



Citation: Matias Gonçalves, L.; Mendoza-Martinez, C.; Alves Rocha, E.P.; Coutinho de Paula, E.; Cardoso, M. Solar Drying of Sludge from a Steel-Wire-Drawing Industry. *Energies* **2023**, *16*, 6314. <https://doi.org/10.3390/en16176314>

Academic Editor: Fabio Montagnaro

Received: 31 July 2023

Revised: 24 August 2023

Accepted: 28 August 2023

Published: 30 August 2023



Copyright: © 2023 by the authors. Licensee MDPI, Basel, Switzerland. This article is an open access article distributed under the terms and conditions of the Creative Commons Attribution (CC BY) license (<https://creativecommons.org/licenses/by/4.0/>).

1. Introduction

Solid-phase water removal treatment of sludge typically comprises the steps of densification, digestion, dewatering, and drying for final use/disposal. As an important fact, sludge treatment always considers volume and mass reduction. The relevant factors that can interfere in the removal of water from the sludge are the distribution, size, shape, and structure of the filter cake; solids concentration; temperature; superficial tension; water fraction; particle load; and compressibility. Thus, the treatment process by which the sludge is produced determines the properties that affect its ability to release water. Typically, excess water in the sludge is removed using a filter press, which is operated under plate and frame pressure (PFP). A feed pump capable of providing a feed pressure and an air compressor capable of providing a press pressure determine the efficiency of the water removal [1].

The sludge contains four types of moisture [2]: (i) free moisture that can be separated by gravitational settling, where thickening is the method of removal; (ii) interstitial water, which is released by mechanical dewatering methods, such as filter press, centrifugation, vacuum filters, and membrane filters, when the flocs are broken or the cells are destroyed; (iii) capillary and bound water that is separated by mechanical dewatering after chemical conditioning; and (iv) hydration water, which is chemically bonded to cell surfaces and

can be released by thermochemical treatments [3]. Diverse methods of industrial sludge management are currently available. Sludge treatments are mainly focused on stabilization, removal of toxic compounds, and volume reduction for value-added applications. This study focuses on volume reduction of sludge that concerns mainly moisture content, which can be as high as 80%.

Among the moisture removal methods, thermal sludge drying is an energy-intensive process, so using solar energy is often the natural first choice due to the competitive cost and environmentally friendly process. Solar drying, despite requiring small investments, presents significant moisture reabsorption by the product in wet periods and incomplete drying, due to the ambient temperature being generally insufficient for this purpose [4]. Artificial dryers promote fast and effective drying (through flow temperature control), despite consuming a considerable amount of energy (fossil, electrical, or otherwise) to heat the drying air. As an alternative, solar dryers, despite being characterized by significant variations in the thermal conditions of the drying air flow (due to the seasonality of solar availability and the randomness of atmospheric attenuation), have a cost of drying that is significantly lower than that of artificial drying (since the solar energy used to heat the airflow has no direct costs) [4]. Furthermore, the implementation of solar energy collectors can help to increase the drying rate to decrease the drying time in some places [5]. Solar drying has potential in the process of drying the sludge from the steel-wire-drawing industry, which is necessary because it allows a reduction in volume and weight for internal or external handling and also co-processing.

Economic development and population growth promote the demand for goods and raw materials, in addition to energy consumption, generating a possible scarcity of natural resources and an increase in the amount of waste generated [6]. The system was formerly linear, with sludge being produced and directed to the landfill. However, the current trend is shifting towards the concept of circular economy [7–10]. The internal or external reinsertion of materials into the production cycle is sought after, aiming to minimize deposition in the environment and consequently avoiding the generation of negative environmental impacts [11–13].

As the linear model of production and consumption of goods intensifies, total global waste generation could reach its peak in this century. According to the report *What a Waste: A Global Review of Solid Waste Management*, published by the World Bank, the generation of urban solid waste has reached about 1.3 billion tons per year in the world [14]. The forecasts made in the report predict that by 2025, waste generation could reach 2.2 billion tons per year [14]. In iron and steel manufacturing processes, various residues are produced, such as slag, mill scale, and sludge. On average, every tonne of steel that is produced generates approximately 200 kg of waste, in scrap metallurgy, or 400 kg in iron-ore-based steel [15]. Mill scale represents 2% and refractories 7% of the total amount of by-products [16].

A technological approach can be applied to solid wastes with various characteristics, but the treatment process depends on the properties of the material to be treated. The main disposal challenge of sludge is directly related to humidity (around 85–90% (wb)) [10]. Thus, several studies have concluded that a drying stage for sludge material is essential before final disposal [17–20], for transportation, handling, and landfilling cost reduction. Thermal drying is a commonly used method for phase separation treatment in the sludge management and reuse process when it is a co-product. The sludge results from equipment involved with the reduction of residual water and gas from different processes. Due to the advancement of the circular economy and environmental requirements, companies have sought to use these wastes in internal processes [16]. Within this context, this article presents a solar drying process for sludge from a wastewater treatment plant (WWTP).

Drying by direct exposure to sunlight is a simple and low-cost alternative for dewatering waste. Solar dryers are a promising alternative to drying by exposure to the sun, as they are designed to save time and maintain product quality. Extensive reviews have been carried out on solar dryers [21–23]. Generally, solar dryers are classified into direct, indirect,

and hybrid solar dryers. In the case of air flow by convection, the classification of solar dryers is into forced (active) and natural (passive). The definition of a direct solar dryer is that the product inside a transparent enclosure is being dried under direct exposure to solar radiation. In the indirect solar dryer, drying is done by natural or forced convection and the product is placed in a drying chamber, where solar energy is absorbed by a collector separate from the drying chamber [21,24]. The hybrid solar dryer combines the characteristics of the direct and indirect types and also uses another heat source in conjunction with solar energy [21,24].

The use of solar energy for drying in Brazil presents a compelling justification for research in the context of sludge. The country's tropical climate offers an abundance of solar resources throughout most of the year [25]. This climatic advantage makes solar drying an attractive and sustainable option for managing various waste streams, including sludge. However, open-air drying causes a risk of environmental pollution, reduces drying efficiency because the waste itself shades the adsorber area, and may affect the properties of the product [26,27]. Indirect forced-circulation solar drying can overcome these problems. Indirect solar drying systems provide better protection to the sludge from external factors and reduce the gases released during drying, due to the enclosed drying chamber. The drying efficiency is enhanced compared to open-air drying due to consistent temperatures and airflow control. Additionally, the dependence on weather conditions is reduced due to greater control design over environmental factors. To the best of our current knowledge, however, there is a lack of sufficient literature reporting on small-scale forced-circulation solar driers for industrial sludge applications.

Figure 1 presents the drying methods in terms of temperature and drying time in a comparative way. According to the research described, in the thermal drying process, the drying temperature can vary from approximately 60 °C to 200 °C. The thermal process can provide faster drying efficiency in a shorter time compared to other drying methods. With this drying method, 100% moisture reduction can be achieved, allowing for 87% weight reduction and 70% volume reduction during the 6 to 10 h drying period. Among the different drying methods, the biostabilization process takes the longest time, but it can reduce the solid residue weight by 85% in 100 days. The drying temperatures of the different drying methods have been reported as 59 ± 37 °C for solar drying, 115 ± 40 °C for thermal drying, 55 ± 15 °C for biodrying, and 58 ± 11 °C for biostabilization [28]. The prototype developed here has an advantage over the studies described, since the time used for solar drying was 6 h, with a reduction of approximately 50% in humidity, operating close to the minimum temperature of approximately 45 ± 7 °C.

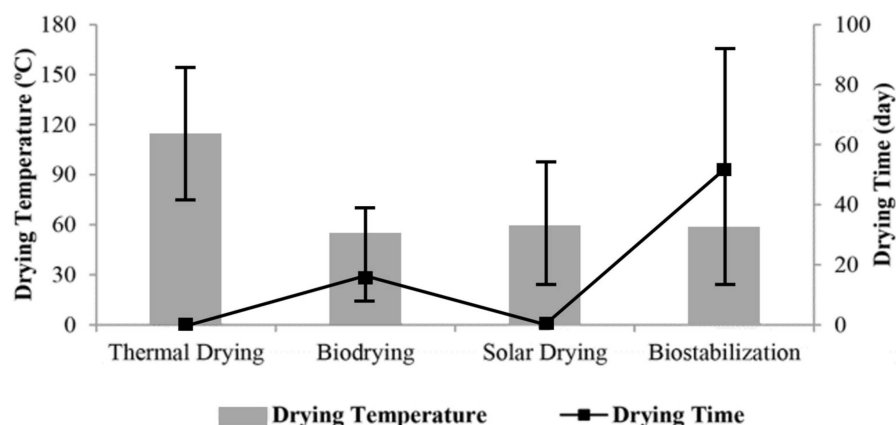


Figure 1. Comparison of drying methods based on drying temperature and drying time [28].

While solar dryers are commonly employed for drying fruits and vegetables, there is a noticeable lack of comprehensive research on the application of solar drying specifically for steel wire sludge. Only one study, conducted by [4], was found on this subject. As the steel industry generates significant volumes of sludge, there is an urgent need for more

research in this area to explore the potential of solar drying technology to address the waste management challenges faced by the steel-wire-drawing industry.

The steel-wire-drawing industry plays an important role for society with products such as electrical wire, cable manufacturing, tension-loaded structural components, springs, paper clips, spokes for wheels, and stringed musical instruments. Surface drawing or shaping is a machining process that uses tensile forces to stretch metal, where the cross section of a wire is reduced by pulling it through a single, or series of, drawing die(s), usually performed at room temperature. The output of this process is known as drawn or cold-drawn wire [29].

As global concern for climate change and sustainable practices continues to grow, adopting solar drying technology aligns with international goals to reduce greenhouse gas emissions and to transition towards more eco-friendly industrial processes. Research in this field can contribute to the development of best practices and guidelines for implementing solar sludge drying systems in steel industries worldwide, promoting the widespread adoption of this responsible technology. Therefore, conducting research on the solar drying of steel-wire-drawing sludge in Brazil and globally is both timely and imperative. The tropical climate of Brazil, with its abundant solar energy resources, provides an ideal setting for exploring the feasibility and efficacy of solar drying technology. Furthermore, addressing the dearth of studies in this specific area will pave the way for sustainable waste management practices, foster economic savings, and contribute to the global effort to combat climate change. There is a need for more research in this area to explore the potential of solar drying technology to address the waste management challenges faced by the steel-wire-drawing industry.

The objective of this research was the construction and testing of an active indirect solar dryer. Experimental data were used to validate the dryer performance, so as to optimize the design parameters. For this purpose, a design of experiment (DOE) employing a quadratic Doehlert model with two factors, temperature and air velocity, was adopted. During the initial phase of this study, the primary goal was to design and assemble the prototype. Then, the WWTP sludge was characterized, and computational fluid dynamics (CFD) software was used to simulate the fluid dynamic air flow within the device. To validate the results, tests were carried out using a thermographic camera and by comparing the observations with the CFD simulation. Lastly, drying tests were performed for calculating the thermal and drying efficiency of the equipment [30,31]. The frame structure of the study is presented in Figure 2.

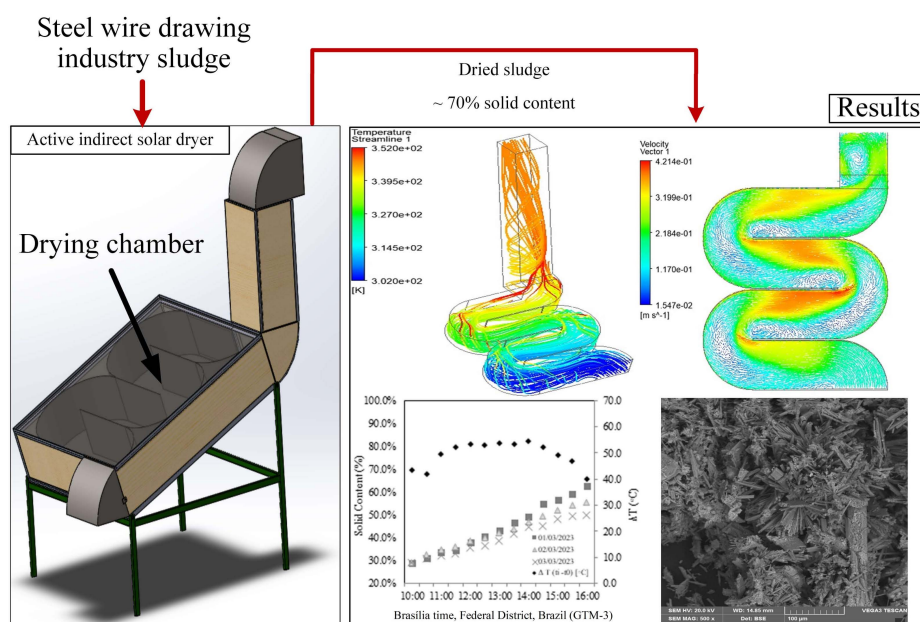


Figure 2. Frame structure of this study.

2. Steel-Wire-Drawing Sludge Production

The drawing process involves reducing the cross-sectional area of the wire by forcing the wire through a conical die. The effluent treatment station's inorganic sludge, known as filter cake in the steel-wire-drawing industry, is generated in the decantation [32]. Typically, inorganic sludge is a mixture of minerals, colloids, and decomposed organic materials. Still, the main compounds are heavy metals in a wide range including copper, cadmium, chromium, lead, mercury, nickel, silver, zinc, platinum, and others [33]. Some studies have used inorganic sludge in value-added applications, for co-products in the manufacturing process [34], which are generally directed to the construction sector [35].

In Brazil, steel wires are commonly applied in different industrial processes, such as civil construction, agrobusiness, metal mechanics, etc. Brazil produces approximately 3.393×10^3 t of steel wire, which represents about 0.09% of Brazil's total crude steel production [36,37]. The extensive production of steel wires generates a significant amount of sludge, which is mainly produced from chemical pickling. The sludge production in Brazil is approximately 245 t/month in a large factory [38]. Due to the challenging disposal, the effluent has a specific control process. The sludge undergoes a neutralization with lime, with subsequent treatment by aeration/oxidation with compressed air, followed by flocculation, decantation, and dewatering in a filter press. The final product is known as filter cake, containing approximately 80% moisture on a wet basis.

Currently, the sludge is sent to a controlled landfill due to its chemical characteristics and quantities, such as an iron content average of 37%, a calcium oxide (CaO) content average of 16%, and other chemical compounds that require specific controls. The pre-treatment of the sludge through a drying process requires other applications [4]. Solar drying presents a good alternative for reducing volume and weight through the drying process because it is based on renewable energy, making the process sustainable.

3. Materials and Methods

The methodology for the development of this study was divided into five stages: collection and characterization of industrial sludge, design and assembly of a hybrid active indirect solar dryer, fluid dynamic analysis of the behavior of the air inside the device using CFD software, tests with a thermographic camera to validate the simulation, and optimization of the sludge drying by calculating the thermal efficiency and drying efficiency of the equipment.

3.1. Sampling

This study used sludge from a steel-wire-drawing plant of ArcelorMittal located in Minas Gerais, Brazil. The filter cake was generated at the treatment facility for effluents from the wire rod and wire treatment processes. The products from this process are the pressing effluent, which returns to the continuous treatment collection tank, and the pressed residue, called WWTP cake.

Sampling was performed after the WWTP pressing process. The collection was carried out in a week of production in the three times of the pressing operation; after pressing, approximately 3 kg was collected and placed in a plastic bag. At the end of the 7 days of sampling, the samples were mixed and homogenized, totaling a sample of 14 kg.

To develop the experiments in this study, a design of experiment (DOE) was performed to evaluate the combined effect of temperature and air velocity by using the response surface method on the drying treatment conditions [39]. A Doehlert model was adopted as the platform of choice for the DOE. As a result, the total number of experiments conducted was 11. Table 1 shows a summary of experimental ranges of the independent variables. Solid yield was the response selected for the proposed design. Each treatment was tested in duplicate. As the design considered two levels for each continuous factor, a quadratic

regression model was used. The predictive polynomial quadratic equation in general form is given by Equation (1).

$$Y = \beta_0 + \sum_{j=1}^k \beta_j X_j + \sum_{j=1}^k \beta_{jj} X_j^2 + \sum_{i < j} \beta_{ij} X_i X_j + \mathcal{E} \quad (1)$$

where Y is the response, β_0 is the intercept coefficient, β_j , β_{ij} , and β_{jj} are the interaction coefficients of the linear, the second-order, and the quadratic terms, k is the number of independent parameters, X_j are the independent variables, and \mathcal{E} is the residual associated to the experiments.

Table 1. Experimental range and values of independent variables used in central composite design.

Independent Variable	Level Variable 1				
Temperature [°C]	−1	−0.5	0	+0.5	+1
	36	43.5	51	58.5	66
	Level Variable 2				
Velocity [mp/s]	−0.866		0		0.866
	1		1.1		1.2

The significance of each term was evaluated based on an analysis of variance (ANOVA) at significance level $\alpha = 0.05$. Results of the DOE model, regression coefficients, and ANOVA can be found in Supplementary Materials File SA.

Temperature control was carried out through digital control of the heat blower, which was possible due to the flow rate, as the fan speed was constant.

3.2. Physicochemical Characteristics of Sludge

The chemical composition of the sludge was obtained by X-ray fluorescence (XRF) in a Philips X'Pert PRO MPD spectrometer (Amsterdam, The Netherlands) and the loss on ignition (LOI) at room temperature. The granulometric distribution was obtained by laser diffraction in a Beckman Coulter LS analyzer LS 13 230, Fraunhofer optical model (Fullerton, CA, USA). In addition, the waste received and pre-treated (crushed + sieved from 100 μm to 200 μm) was coated with gold and observed by scanning electron microscopy SEM, Hitachi high-tech S-4100, accelerating voltage of 5 kV and 25 kV (Tokio, Japan). Mill scale X-ray diffraction (XRD) analyses, at room temperature and calcined, were performed using a Malvern Panalytical X'Pert MRD diffractometer Ni-filtered CuK α radiation, PIXcel 1D detector, and exposure corresponded to about 2 s per step of 0.02 2θ at room temperature (Malvern, United Kingdom).

The sludge sample was classified according to the NBR 10004 standard [40]. The samples showed concentrations of lead, iron, calcium, and chlorine higher than the limits established for the solubilization test. Thus, steel wire sludge was classified as class II waste—non-inert; the results can be found in Supplementary Materials File SB.

3.3. Development of Hybrid Solar Dryer

The proposed dryer had a drying tray with an area of 0.108 m² (0.24 m \times 0.45 m). The drying capacity of the dryer was approximately 4 kg of wet product for every 1 m² of drying area [41]. A small-scale active indirect solar dryer was developed as shown in Figure 3. The wooden cabin structure was covered by 0.008 m thick tempered glass, externally coated with galvanized steel sheets, with rock wool insulation. Matte black was used to paint the dryer structure to increase the absorption of solar radiation. The solar dryer dimensions were 1.15 m L \times 1.25 m W \times 0.25 m H in the heating channel and 0.24 m L \times 0.24 m W \times 0.45 m H in the drying chamber, with total areas of 0.408 m² and 0.108 m² for the drying chamber and solar collector, respectively. Drying capacity was estimated at approximately 2 kg of wet sludge per batch. The air flow was carried out by convection forced by a fan at the inlet. The development of drying kinetics with solar

energy on a laboratory scale allows designing a new prototype on an industrial scale. In the steelmaking process, it is estimated that for each ton of steel, a typical steelworks generates approximately 0.6 tons of waste [29].

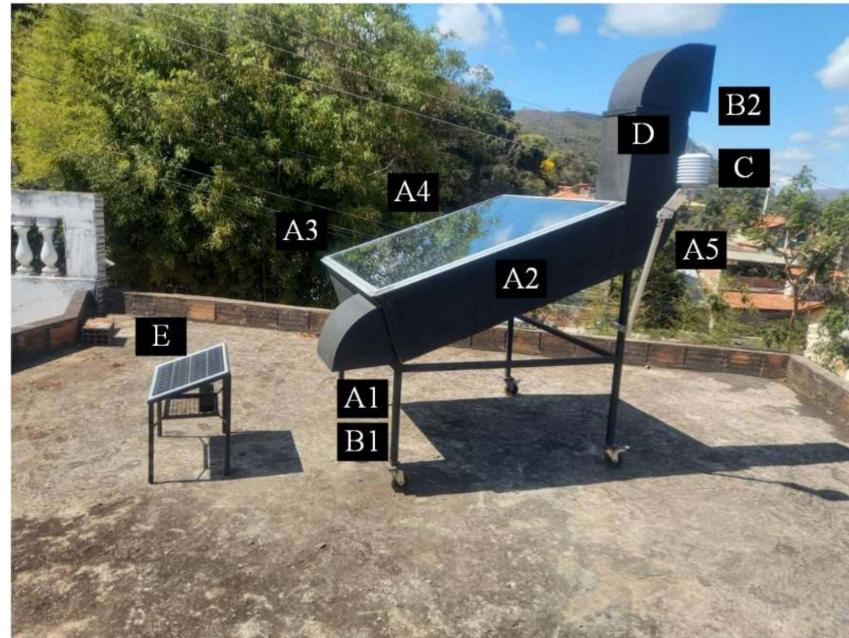


Figure 3. Picture of the active indirect solar dryer: (A1, A2, A3, A4, and A5) PT-100 temperature sensors, (B1 and B2) thermo-hygrometer, (C) pyranometer, (D) anemometer, (E) photovoltaic panel.

The entire structure was made with 20 mm × 30 mm metal sheets fixed to 1" × 1/8" angle brackets. The coating for mechanical resistance and thermal insulation was carried out by using marine MDF with a thickness of 13 mm filled with a 12 mm ceramic fiber blanket with a capacity for thermal insulation of 1260 °C. The dryer was fixed with interlocking plates without the use of screws, in order to guarantee its sealing. The drying basket was made of aluminum fixed with aluminum rivets, with 4 compartments of (270 × 230) mm. The upper cover was built in aluminum H profile, exceeding the side strip by 30 mm, allowing movement for alteration and/or cleaning of the equipment interior. In addition, these edges were misaligned with the smaller area on the top of the dryer, preventing the entry of moisture from the external environment. The lid was made of 8 mm thick low-Fe tempered glass. The baffle was also built with 20 mm × 30 mm metal fixed to the absorber plate painted in matte black for greater absorption of solar radiation.

Partial incidence of solar radiation could pass through the glass cover and reach the absorber plate. The hot air flow removed water from the product and exited the dryer through a rectangular screened section. The product was inserted and removed from the dryer through the side door. The dryer was positioned with an inclination angle of 20° facing north. The tilt angle was defined as the absolute value of the local latitude in order to maximize the average annual efficiency [42]. The experiments were carried out over four days in November (spring season in the Earth's southern hemisphere). To assess the influence of weather conditions on the fluid dynamic behavior of heated air, four tests were performed. During the experiments, incident solar radiation, ambient temperature and relative humidity, exit velocity, and inlet and outlet temperatures were recorded. The photovoltaic panel allowed the system to be autonomous, but on an industrial scale, process variables such as particulate matter would reduce the efficiency of electricity generation for the fan responsible for the forced convection of the equipment. In this case, a dedusting process would be necessary, either by an automated or manual system. The solar dryer and panel must be installed in an open area to capture solar radiation. The sensors used in the

experimental drier prototype are represented in Figure 1 and detailed in Supplementary Materials File SD.

3.4. Computational Fluid Dynamics (CFD)

CFD software deals with the numerical simulation of fluid flow, heat transfer, and associated phenomena. This simulation can be fundamental in dimensioning processes and in understanding the behavior of fluids to help understand processes and equipment, which for the current project was complementary software.

CFD is a technique used to solve and/or numerically simulate differential equations of conservation of mass, energy, and momentum for flow problems in general by means of the finite volume method [43]. Its application basically consists of three steps: (i) Preprocessing: The geometry of the computational domain that represents the region or equipment in which the flow must be represented is defined. Then, the domain is discretized into a large number of regular geometry elements called the computational mesh. Finally, the boundary conditions, physical models, physical characteristics of the materials and fluids considered, and numerical parameters necessary for the iterative solution of the equations are defined; (ii) Processing: The simulation is processed through iterative calculations; (iii) Post-processing: The results are visualized through profiles, contour lines, flow lines, and surfaces for variables such as velocity, pressure, temperature, and concentration. The differential equations of conservation of mass, momentum, and energy that were to be solved via CFD in this project are presented in Equations (2)–(4), respectively:

$$\frac{\partial \rho}{\partial t} + \frac{\partial(\rho u_i)}{\partial x_i} = 0 \quad (2)$$

$$\frac{\partial(\rho u_i)}{\partial t} + \frac{\partial(\rho u_i u_j)}{\partial x_j} = -\frac{\partial p}{\partial x_i} + \frac{\partial}{\partial x_j} \left[\mu \left(\frac{\partial u_i}{\partial x_j} + \frac{\partial u_j}{\partial x_i} \right) + \delta_{ij} \lambda \frac{\partial u_i}{\partial x_j} \right] + \rho g_i + S_{mom} \quad (3)$$

$$\frac{\partial(\rho h)}{\partial t} + \frac{\partial(\rho u_i h)}{\partial x_i} + \frac{\partial p}{\partial x_i} = \frac{\partial}{\partial x_i} \left(k_T \frac{\partial t}{\partial x_i} + \frac{\mu}{Pr} \frac{\partial h}{\partial x_j} S_E \right) \quad (4)$$

where p represents the pressure, ρ represents the specific mass, h the enthalpy, μ represents the dynamic viscosity, k represents the thermal conductivity, Pr represents the Prandtl number, and t the time; and finally u , which represent the fluid velocities in the x directions, respectively.

In this project, CFD simulations were carried out to analyze and evaluate different geometric arrangements and operating configurations through velocity, pressure, and temperature profiles, among others, for the various cases of interest to be studied [44,45]. The results obtained were used to aid in the dimensioning and design of prototypes on a laboratory scale in order to enable the definition of the most suitable project for the dryer on a pilot or industrial scale.

3.5. Thermographic Analysis

For a comparative analysis with CFD, non-contact thermography was used. This non-invasive technique aimed to detect the distribution of thermal energy emitted by the drier and sample surface by radiation. It is capable of detecting, visualizing, and recording different levels of temperature distribution across the surface of an object. Non-contact thermography allows the study of the temperature of bodies, through the infrared radiation emitted by them using a thermographic camera [46]. This technique has some advantages over other temperature measurement systems, namely, those that use contact techniques: fast response time, being able to follow transient temperature phenomena, high precision, high repeatability, and reliability of measurements [46,47].

To validate the CFD simulation, thermographic analysis was performed, which is a non-invasive inspection technique. This method is based on the detection of infrared

radiation emitted by bodies that have intensity proportional to their temperatures. The equipment used was a FLIR Systems T420 thermographic camera (Wilsonville, OR, USA). Thermographic images of the solar dryer allowed the verification of thermal anomalies, whereby it was possible to verify at which point the highest distribution of temperatures occurred during the drying tests. In addition to the analyses of the structure of the equipment, images of the samples were also taken during the drying process. In the samples, the distribution of heat in the area of the drying trays filled with the studied residue was analyzed [48]. The thermographic images, with image recordings every 30 min during the drying process, provided the thermal profile of the solar dryer.

3.6. Drying Process

The drying tests of the steel-drawing sludge in the solar dryer were carried out in November, from 10 a.m. to 4 p.m., Brasilia time, Federal District, Brazil (GTM-3). The reduction of moisture in the samples was monitored by means of weighing at regular intervals of 30 min. The sludge was loaded through 4 trays that held 0.5 kg each being placed in the drying nap that is inside the chimney of the equipment, for a total load of 2 kg of sludge for 6 h of drying. The prototype was developed on a laboratory scale that would not allow its incorporation into an industrial process. The construction cost was approximately USD 502.00, being designed and built in approximately 4 months. The project can serve as a basis for designing equipment for the drying process in the steel-wire-drawing industry. When the residues in the solar dryer reached hygroscopic equilibrium, the moisture content was measured. Curves representing the relationship between drying time and moisture content were derived based on the moisture content at the end and during each drying time interval.

The thermal efficiency of the dryer was calculated using Equation (5) [41]. The ambient temperature, inlet airflow humidity and temperature, outlet air velocity and humidity, and incident solar radiation were measured with k-type thermocouples (maximum uncertainty of ± 0.6 °C), thermometer-hygrometers RH520 ($\pm 3\%$ uncertainty for humidity and ± 1 °C for temperature), a thermo-anemometer THAL 300 (uncertainty of $\pm 3\%$ for each parameter), and a precision spectral pyranometer (PSP) (uncertainty of $\pm 1\%$) connected to an A1201 squitter data acquisition system. Uncertainty analysis was performed according to a 95% confidence interval to estimate the errors in the experimental results [41].

$$\eta_T = \frac{\dot{m}(h_{in} - h_{out})}{A \cdot G} \quad (5)$$

where \dot{m} is the mass flow of air, h_{in} and h_{out} are the specific enthalpies of the dryer inlet and outlet, respectively, A is the collector area, and G is the hemispherical area of solar radiation in the collector plane.

Four trays within the drying chamber were filled with sludge samples, each weighing 500 g. During the tests, the temperature and relative humidity of the air at the inlet and outlet of the dryer (using two thermo-hygrometers), the air velocity at the inlet of the dryer (using an anemometer), and solar radiation (using a pyranometer) were measured. For each solar drying test, determinations of drying curves, energy balance, and thermal drying and device efficiency were carried out.

As shown in Equation (6), the drying efficiency (η_s) was calculated by the ratio between the vaporization energy of the product water and the energy required by the dryer [41].

$$\eta_s = \frac{\int \dot{m}_{H_2O} \cdot h_{lv} \cdot dt}{\int A \cdot G \cdot dt} \quad (6)$$

where \dot{m}_{H_2O} is the instantaneous flow of moisture that is withdrawn from the product in the dryer, and h_{lv} is the latent heat of vaporization.

4. Results and Discussion

4.1. Sludge Characterization

4.1.1. X-ray Diffraction

One of the techniques used to characterize the sample was X-ray diffraction; the analysis detected the presence of iron oxide (Fe_2O_3). The major element observed was iron (Fe), the minor elements were sulfur (S), carbon (C), and calcium (Ca), and the trace elements were oxygen (O), sodium (Na), silicon (Si), and chloride (Cl); these are shown in Figure 4. The excessive amounts and forms of these elements may cause negative environmental impacts. However, until now, steel-wire-drawing sludge is being sent to controlled landfills, generating transport costs and damage to the environment. Additional information about the elements found in the sludge sample are summarized in Supplementary Materials File SC.

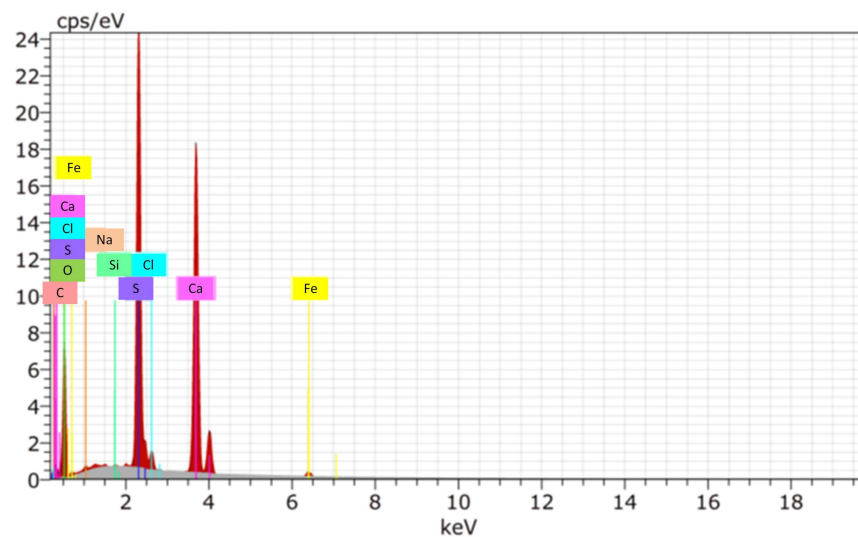


Figure 4. X-ray diffractogram of the steel-wire-sludge sample.

Due to the presence of iron in the composition of the inorganic sludge, its possible destinations become restricted; some researchers have sought to incorporate it into ceramic materials to replace a percentage of conventional aggregates [49]. Therefore, the use of industrial sludge in lightweight aggregates not only provides ways to reuse industrial sludge but also reduces the consumption requirements for sintering lightweight aggregates [50].

4.1.2. SEM Analysis

In the SEM analysis, shown in Figure 5, the two figures showed heterogeneous morphology. They featured different types of particles from narrow to large size.

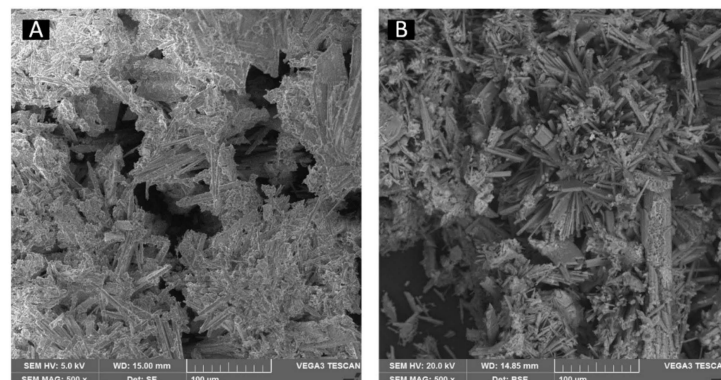


Figure 5. SEM images of the raw sludge sample at ambient temperature. (A) 100 µm field of view and 5 kV accelerating voltage. (B) 100 µm field of view and 20 kV accelerating voltage.

The microstructure of the sludge at room temperature showed different porosity trends and different surface morphologies. Figure 5A shows the appearance of coarse grains and the formation of glassy phases. However, it has a different morphology characterized by the appearance of coarse grains. And, Figure 5B presents a format that allows viewing the heterogeneity of the structure and non-conforming parts. This becomes possible with voltage acceleration from 5 kV to 20 KV, which better details the sample surface.

4.2. CFD Analysis Results

The CFD simulations were carried out with the objective of analyzing and evaluating different geometric arrangements and operational configurations, through velocity and temperature profiles, for the different tests carried out. The results helped in the study of the fluid dynamic behavior of the air inside the equipment. Figure 6 presents a comparison of the thermal profiles of simulations for four different angles of the baffle located inside the equipment. Details of the CFD simulation stage of the solar dryer prototype are presented in Supplementary Materials File SE.

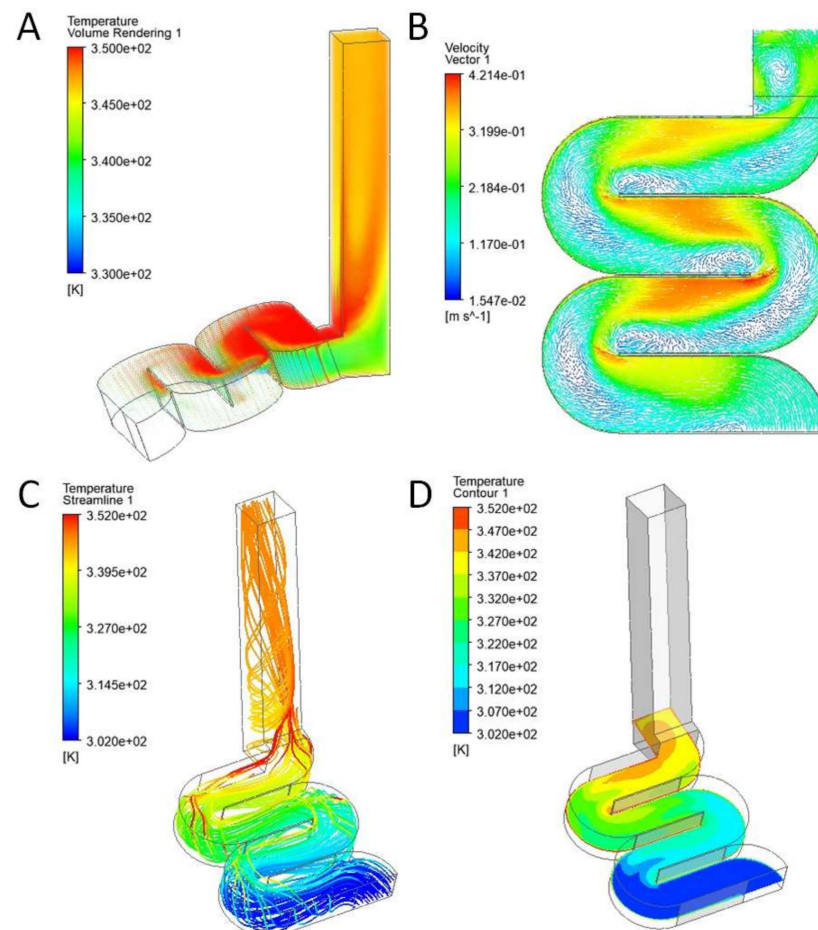


Figure 6. CFD simulation images of the solar dryer. (A) Temperature as a function of air volume; (B) temperature as a function of the velocity vector; (C) temperature as a function of simplified volume; (D) temperature depending on the baffle.

The results obtained from Figure 6A demonstrate a remarkable increase in temperature along the baffle channels, which is responsible for increasing the residence time of the air and consequently increasing the thermal efficiency of the device. This increase in residence time contributes to enhancing the thermal efficiency of the device, ensuring optimal performance of the solar dryer. The heated air effectively traverses the upper part of the baffle and converges towards the center of the drying section, creating a homogeneous temperature profile conducive to efficient drying.

Additionally, Figure 6B exhibits a temperature increase along the baffle channel, with a tendency for the air to concentrate towards the center of the channel. The venturi effect observed at the beginning of each channel results from the change in air behavior as it passes through a larger area.

Furthermore, Figure 6C highlights the proportional relationship between the increase in air velocity and temperature gain, demonstrating the well-designed fluid dynamics within the solar dryer. As the air reaches the end of the baffle channel, it encounters the drying basket filled with sludge, causing resistance to the airflow. Nevertheless, the heated air adeptly permeates the sludge samples in a turbulent manner, facilitating efficient moisture removal. Lastly, Figure 6D portrays the dynamic temperature changes along the channel, with the air starting at its minimum temperature and gradually reaching its highest temperature by the end of the baffle. This temperature rise is attributed to efficient heat exchange through conduction and convection with the matte black plate situated inside the solar dryer.

Overall, these observations not only validate the effectiveness of the active indirect solar dryer but also provide valuable insights into the intricate thermal and fluid dynamics involved. Such knowledge is vital for designing and optimizing similar drying technologies for various applications worldwide, paving the way for sustainable and environmentally friendly waste management practices across industries.

4.3. Thermographic Analysis

To validate the CFD simulation, a non-invasive analysis was performed with a thermographic camera. The boundary conditions of the CFD simulation were the same as the thermographic analysis, as shown in Figure 7. The temperature was intrinsically correlated with the fraction of mass and/or the volume of water (humidity) where the enthalpy (h) was the amount of energy found in the air flow of the drying process. Thermographic analyses of the sludge samples made it possible to investigate and compare their thermal behavior according to the variables of the drying process. The images were taken at three drying times on two different days, at 10:00 a.m., 12:00 p.m., and 4:00 p.m. on 28 March 2023, corresponding to Figure 7A–C, respectively, and at the same times on 29 March 2023, corresponding to Figure 7D–F, respectively.

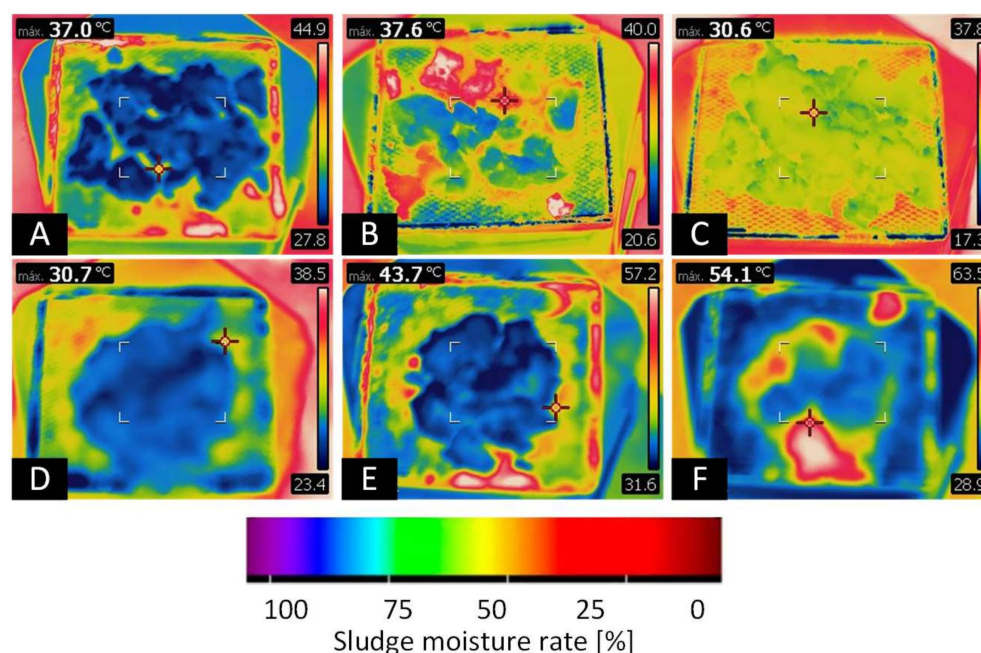


Figure 7. CFD simulation images of inorganic sludge samples: (A) 70% humidity, (B) 61.2% humidity, (C) 34.5% humidity, (D) 70% humidity, (E) 62.5% humidity, (F) 30.4% humidity.

In the drying tests carried out on 28 March 2023, in Figure 7A at 10 a.m., a homogeneous distribution of moisture can be seen throughout the material studied. Heat transfer to the sample occurred from the edges to the center. Figure 7B at 12 a.m. already had a smaller diameter of wet material, with a higher concentration of heat by conduction in the lower area. The Figure 7C at 4 p.m. had reduced its moisture to about 50%, with some scattered points in blue color with a small percentage of wet material.

In the drying tests carried out on 29 March 2023, in sample 7D at 10 a.m., a homogeneous distribution of moisture concentrated in the center of the drying tray can be seen. Heat transfer to the sample occurred from the edges to the center with a predominance of heat transfer by conduction. Figure 7E at 12 a.m. already had a smaller diameter of wet material, with a homogeneous moisture reduction from the edges to the center. Finally, the Figure 7F at 4 p.m. was almost dry, with some dots distributed in the center of the tray in blue.

Figure 8 shows the tests carried out in the solar dryer prototype under conventional (only with solar radiation) and hybrid mode (air heated by solar radiation coupled to a secondary heat source from a heat blower). In this case, thermographic analysis was simulating the temperatures of heat leaks in industrial processes.

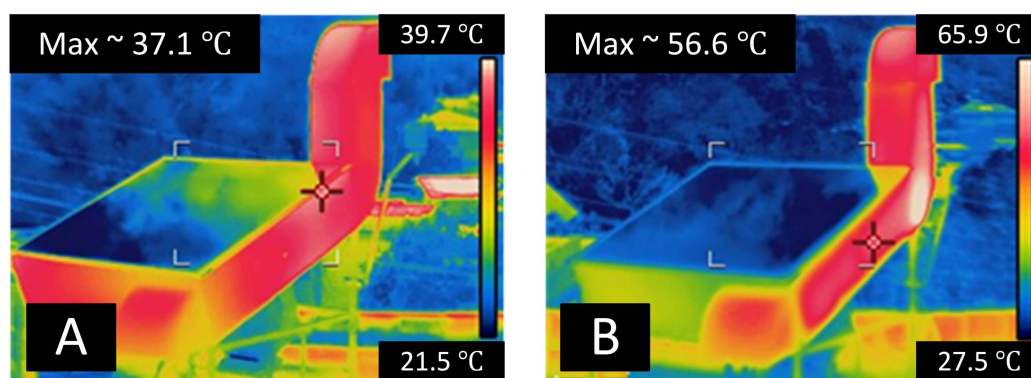


Figure 8. Thermal images of the solar dryer. (A) Conventional drying and (B) hybrid drying.

A thermographic image of the solar dryer was highlighted in the drying chamber that is located below the chimney of the equipment, which shows overheating in red. However, the structure of the dryer had a uniform temperature on the surface, with a lower incidence of thermal radiation. The temperature was intrinsically correlated with the fraction of mass and/or the volume of water (humidity) where the enthalpy (h) was the amount of energy found in the air flow of the drying process.

4.4. Results of Drying Tests

The testing phase occurred during the transition from winter to spring, coinciding with the onset of the rainy season in Brazil. This period represents intermediate environmental conditions in that country. As the rainy season commences, the air's relative humidity rises, leading to varying drying conditions. This enables comparisons across different ranges of relative humidity. Figure 9 summarizes the observations for hemispheric solar radiation, mass air flow inside the device, thermal efficiency, outlet air temperature, and the drying curve during the experimental drying.

The drying test variables observed for Brazilian steel-wire-drawing sludge revealed the significant influence of climate conditions and solar radiation on the performance of the solar dryer. The fluctuations in ambient temperature caused by cloud cover and solar radiation variations throughout the day made it challenging to maintain a constant global solar radiation value (Figure 9A). The period of greatest solar incidence occurred between 10 a.m. and 2 p.m., in accordance with [51].

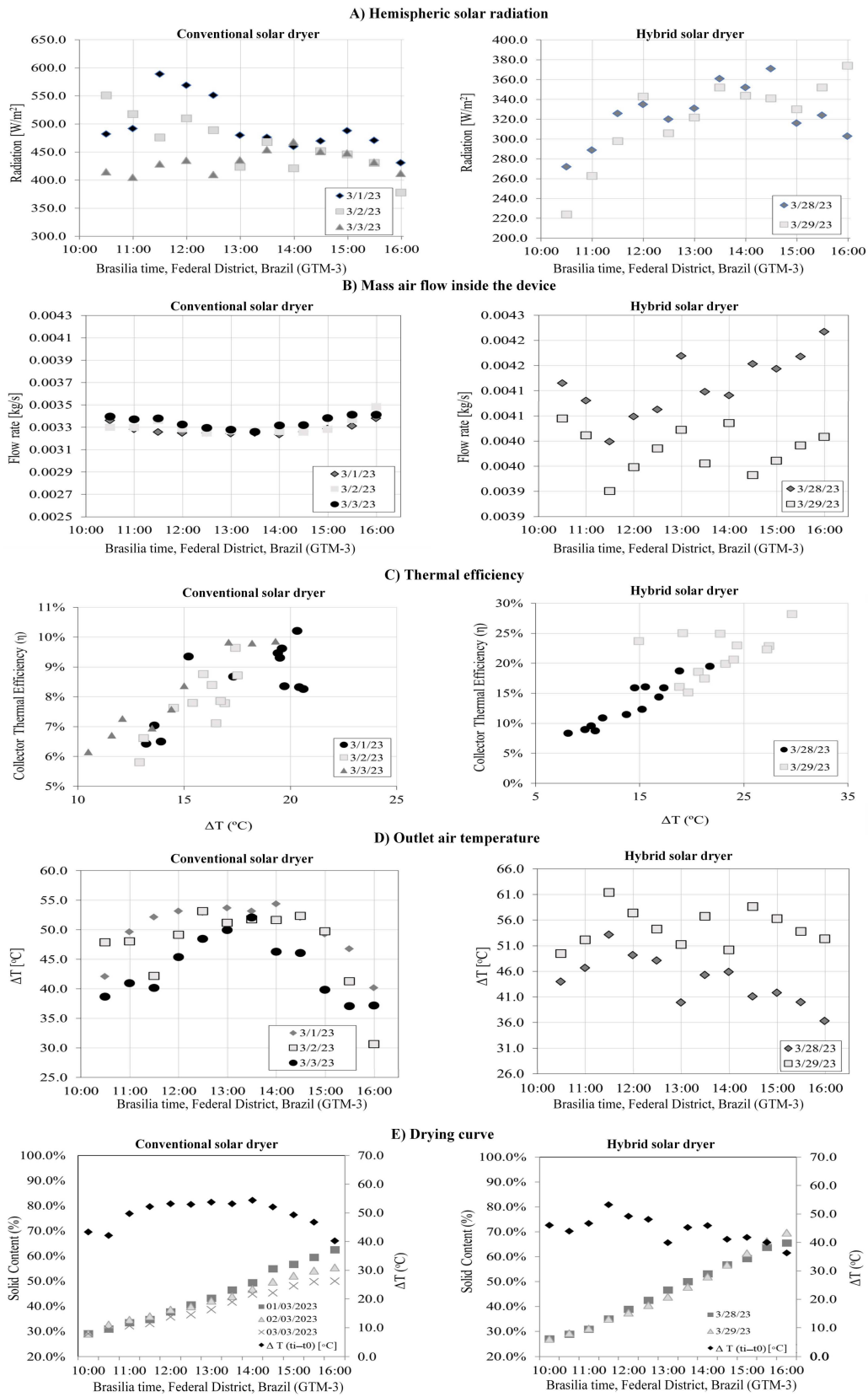


Figure 9. Drying test variables observed for Brazilian steel-wire-drawing sludge.

Figure 9B shows a greater oscillation in the thermal efficiency at higher temperatures, due to the greater availability of incident solar radiation in the plane of the dryer. High thermal efficiency promotes an increase in the internal temperature of the device’s airflow. At lower

temperatures, variations in thermal efficiency are smaller, as the response time to weather conditions influences the variables on a smaller scale. The highest temperatures achieved in the dryer correlated with the highest solar incidence, and reductions in incident solar radiation led to proportional decreases in internal equipment temperature, as shown in Figure 9C. The implementation of a heat reserve mechanism could mitigate such fluctuations.

Furthermore, the drying curve presented in Figure 9D indicated greater attenuation in the first hours of testing, resulting in enhanced removal of surface water from the residue, according to the drying standards as observed in Figure 9E. The average radiation incident on the plane of the device and average ΔT were around $343.0 \pm 1.0 \text{ W/m}^2$ and $30.7.0 \pm 0.6 \text{ }^\circ\text{C}$, and $589.0 \pm 1.0 \text{ W/m}^2$ and $54.4 \pm 0.6 \text{ }^\circ\text{C}$, for conventional and hybrid solar dryers, respectively. The instantaneous thermal efficiency of the no-load solar dryer ranged from 8.4% to 28.2% in the test performed according to climatic variations. The results of the drying test conducted on 1–3 March 2023 with the hybrid solar dryer, with 29% for the initial solid mass, reached 62.5% for the solid mass by the test's end. Two days of tests were carried out on March 28 and 29 of the year 2023, starting with a solids mass of 27%, and by the end of the tests an average of 69.6% for the final solids mass was obtained.

The implementation of the solar dryer could lead to significant cost savings in the transport of steel-wire-drawing sludge, potentially reducing costs by up to 30.4%. By removing water through the solar drying process, the weight and volume of the sludge decreases, translating to considerable cost reductions. With an average generation of 245 tons per month of sludge with approximately 30.4% moisture content and a final cost of USD 1960.00, a potential monthly savings of up to USD 595.84 could be achieved, considering the cost of USD 8.00 per ton for the sludge delivered to the transporter.

Overall, these findings underscore the economic viability and environmental benefits of adopting solar drying technologies for managing steel industry waste, providing a pathway for worldwide applications and enhancing sustainable waste management practices across industries.

The adoption of solar sludge dryers in Brazil and worldwide would offer numerous benefits. Firstly, it could substantially reduce the environmental impact of waste disposal by minimizing the volume of sludge generated and enhancing the solid material content through moisture reduction. This, in turn, would reduce the reliance on conventional landfilling methods, contributing to a more sustainable waste management approach. Secondly, solar drying presents a cost-effective and energy-efficient alternative compared to traditional drying methods. As solar energy is readily available in Brazil and many other regions around the world, harnessing this renewable resource for drying processes can lead to significant savings in energy costs and operational expenses.

5. Conclusions

This paper highlights the significance of adopting solar-energy-based drying technologies for processing filter cake from the steel-wire-drawing process. The hybrid solar dryer displayed notable efficiency when compared to conventional equipment. Notably, the outer layer of the sludge samples demonstrated the highest percentage of moisture removal, indicating effective drying results.

Throughout the drying tests, the solar dryer exhibited substantial improvements in solid material content, with an increase from 29% to 62.5% in the first three days of testing in conventional mode. Moreover, in the last two days of testing, the solid material content increased from 27% to an impressive 69.6%. This demonstrated the capability of the developed prototype to significantly reduce moisture content in the sludge.

The thermal efficiency achieved during all tests was approximately 30%, underlining the effectiveness of the solar drying process. These findings hold broad implications transcending the specific scenarios tied to steelmaking sludge treatment:

- (a) Circular economy solutions must be reinforced to mitigate potential negative impacts on economic, energy, sustainability, and scalability aspects resulting from wastewater treatment plant updates.

- (b) The integration of multiple drying technology upgrade solutions utilizing solar energy will be pivotal in minimizing environmental impacts and addressing any shortcomings in selected technological solutions concerning economy, energy, sustainability, and scalability.

In conclusion, the strategic application of innovative solar-based approaches to drying scenarios can substantially expedite the accomplishment of solid waste disposal targets in steel industries worldwide. The general applicability of these insights underscores the global relevance of adopting such practices to foster sustainable and efficient waste management across the steel sector.

Supplementary Materials: The following supporting information can be downloaded at: <https://www.mdpi.com/article/10.3390/en16176314/s1>, Supplementary Material File SA: Process performance modeling. Supplementary Material File SB: Elemental composition of steel wire sludge using X-ray diffraction analysis. Supplementary Material File SC: Details of the development of the solar dryer. Supplementary Material File SD: Elements detected in steel wire sludge structure. Supplementary material File SE: Details of the CFD simulation stage of the solar dryer prototype.

Author Contributions: Conceptualization, Methodology, Formal analysis, Data curation, Investigation, Writing—original draft, Visualization, L.M.G.; Conceptualization, Visualization, Investigation, Writing—original draft, Writing—reviewing and editing, C.M.-M.; Conceptualization, Methodology, Data curation, Investigation, Writing—original draft, Writing—reviewing and editing, E.P.A.R.; Supervision, Writing—reviewing and editing, E.C.d.P.; Supervision, Writing—reviewing and editing, M.C. All authors have read and agreed to the published version of the manuscript.

Funding: This research received no external funding.

Data Availability Statement: The data shown in this work was produced experimentally and has been shown in the manuscript and Supplementary files.

Acknowledgments: The authors thank Wander dos Santos Luz from ArcelorMittal for kindly collecting the feedstock material for this study.

Conflicts of Interest: The authors declare no conflict of interest.

Nomenclature

WWTP	Wastewater treatment plant
DOE	Employing a quadratic Doehlert
CFD	Computational fluid dynamics
PFP	Plate and frame pressure
PSP	Precision spectral pyranometer
A	Area, m ²
C _p	Specific heat capacity, J/kg.K
G	Hemispheric solar radiation, W/m ²
h _i	Specific air inlet enthalpy, J/kg
h _o	Specific enthalpy of air exit, J/kg
m _i	Initial mass of solid waste sampling, kg
m _f	Final mass Final mass of solid waste sampling, kg
m _x	Instantaneous mass of solid residue over the process time, kg
T _i	Collector inlet air temperature, °C
T ₀	Collector outlet air temperature, °C
T _a	Ambient air temperature, °C
U _{i(BU)}	Initial moisture content on a wet basis, %
U _{x(BU)}	Instant moisture content on a wet basis, %
\dot{m}	Air mass flow, kg/s
η	Drying efficiency, %
η _i	Instant solar dryer efficiency, %

References

1. Cui, Y.; Zhu, W.; Wu, S.; Liu, J.; Hou, H.; Lin, N. The role of lime in dredged mud dewatered by a plate and frame filter press and potential substitutes. *Environ. Sci. Pollut. Res.* **2021**, *28*, 17331–17342. [[CrossRef](#)]
2. Vesilind, P.A.; Martel, C.J. Freezing of Water and Wastewater Sludges. *J. Environ. Eng.* **1990**, *116*, 854–862. [[CrossRef](#)]
3. Mowla, D.; Tran, H.; Allen, D.G. A review of the properties of biosludge and its relevance to enhanced dewatering processes. *Biomass Bioenergy* **2013**, *58*, 365–378. [[CrossRef](#)]
4. Ferreira, A.G.; Gonçalves, L.M.; Maia, C.B. Solar drying of a solid waste from steel wire industry. *Appl. Therm. Eng.* **2014**, *73*, 104–110. [[CrossRef](#)]
5. Di Fraia, S.; Figaj, R.D.; Massarotti, N.; Vanoli, L. An integrated system for sewage sludge drying through solar energy and a combined heat and power unit fuelled by biogas. *Energy Convers. Manag.* **2018**, *171*, 587–603. [[CrossRef](#)]
6. Vilarinho, I.S.; Lopes, A.L.; Carneiro, J.; Pinto, C.; Labrincha, J.A.; Seabra, M.P. A New Added-Value Application for Steel Wire Drawing Mill Scale Waste in Stoneware Ceramic Products. *Metals* **2021**, *11*, 661. [[CrossRef](#)]
7. Moschen-Schimek, J.; Kasper, T.; Huber-Humer, M. Critical review of the recovery rates of construction and demolition waste in the European Union—An analysis of influencing factors in selected EU countries. *Waste Manag.* **2023**, *167*, 150–164. [[CrossRef](#)]
8. Stander, H.-M.; Cohen, B.; Harrison, S.T.; Broadhurst, J.L. Validity of using expert judgements to inform multiple criteria decision analysis: Selecting technologies for sulfide-enriched fine coal waste reuse. *J. Clean. Prod.* **2023**, *415*, 137671. [[CrossRef](#)]
9. Morgan, A.; Vicenç, A.; Lluís, C.; Ignasi, R.R.; Wolfgang, G. Strategic Routes for Wastewater Treatment Plant Upgrades to Reduce Micropollutants in European Surface Water Bodies. *J. Clean. Prod.* **2023**, *415*, 137867. [[CrossRef](#)]
10. Lum, M.M.X.; Ng, K.H.; Lai, S.Y.; Mohamed, A.R.; Alsultan, A.G.; Taufiq-Yap, Y.H.; Koh, M.K.; Mohamed, M.A.; Vo, D.-V.N.; Subramaniam, M.; et al. Sulfur dioxide catalytic reduction for environmental sustainability and circular economy: A review. *Process. Saf. Environ. Prot.* **2023**, *176*, 580–604. [[CrossRef](#)]
11. Hagedorn, W.; Jäger, S.; Wieczorek, L.; Kronenberg, P.; Greiff, K.; Weber, S.; Roettger, A. More than recycling—The potential of the circular economy shown by a case study of the metal working industry. *J. Clean. Prod.* **2022**, *377*, 134439. [[CrossRef](#)]
12. Somani, M.; Hölzle, I.; Datta, M.; Ramana, G. An investigation on mobility of heavy metals for assessing the reusability of soil-like material reclaimed from mining of municipal solid waste dumpsites. *Waste Manag.* **2023**, *167*, 113–121. [[CrossRef](#)] [[PubMed](#)]
13. Dong, Y.; Xu, F.; Liang, X.; Huang, J.; Yan, J.; Wang, H.; Hou, Y. Beneficial use of dredged sediments as a resource for mine reclamation: A case study of Lake Dianchi's management in China. *Waste Manag.* **2023**, *167*, 81–91. [[CrossRef](#)] [[PubMed](#)]
14. Hoornweg, D.; Bhada-Tata, P.; Kennedy, C. Peak Waste: When Is It Likely to Occur? *J. Ind. Ecol.* **2015**, *19*, 117–128. [[CrossRef](#)]
15. Branca, T.A.; Colla, V.; Algermissen, D.; Granbom, H.; Martini, U.; Morillon, A.; Pietruck, R.; Rosendahl, S. Reuse and Recycling of By-Products in the Steel Sector: Recent Achievements Paving the Way to Circular Economy and Industrial Symbiosis in Europe. *Metals* **2020**, *10*, 345. [[CrossRef](#)]
16. Colla, V.; Branca, T.A.; Pietruck, R.; Wölfelschneider, S.; Morillon, A.; Algermissen, D.; Rosendahl, S.; Granbom, H.; Martini, U.; Snaet, D. Future Research and Developments on Reuse and Recycling of Steelmaking By-Products. *Metals* **2023**, *13*, 676. [[CrossRef](#)]
17. Peregrina, C.; Rudolph, V.; Lecomte, D.; Arlabosse, P. Immersion frying for the thermal drying of sewage sludge: An economic assessment. *J. Environ. Manag.* **2008**, *86*, 246–261. [[CrossRef](#)]
18. Kelessidis, A.; Stasinakis, A.S. Comparative study of the methods used for treatment and final disposal of sewage sludge in European countries. *Waste Manag.* **2012**, *32*, 1186–1195. [[CrossRef](#)]
19. Bennamoun, L.; Arlabosse, P.; Léonard, A. Review on fundamental aspect of application of drying process to wastewater sludge. *Renew. Sustain. Energy Rev.* **2013**, *28*, 29–43. [[CrossRef](#)]
20. Martinez, C.L.M.; Sermyagina, E.; Vakkilainen, E. Hydrothermal Carbonization of Chemical and Biological Pulp Mill Sludges. *Energies* **2021**, *14*, 5693. [[CrossRef](#)]
21. Mustayen, A.; Mekhilef, S.; Saidur, R. Performance study of different solar dryers: A review. *Renew. Sustain. Energy Rev.* **2014**, *34*, 463–470. [[CrossRef](#)]
22. Lingayat, A.; Balijepalli, R.; Chandramohan, V. Applications of solar energy based drying technologies in various industries—A review. *Sol. Energy* **2021**, *229*, 52–68. [[CrossRef](#)]
23. VijayaVenkataRaman, S.; Iniyan, S.; Goic, R. A review of solar drying technologies. *Renew. Sustain. Energy Rev.* **2012**, *16*, 2652–2670. [[CrossRef](#)]
24. Prakash, O.; Kumar, A. Historical Review and Recent Trends in Solar Drying Systems. *Int. J. Green Energy* **2013**, *10*, 690–738. [[CrossRef](#)]
25. Nascimento, C.J.D.; Oliveira, M.H.d.S.; Santos, D.d.C.; de Lima, T.L.B.; Leite, D.D.d.F.; Ferreira, J.P.d.L.; de Figueirêdo, R.M.F.; Feitosa, J.P.C.; Lara, E.Z. Solar drying of residue from Brazil nut processing. *Braz. J. Food Technol.* **2021**, *24*, 24. [[CrossRef](#)]
26. Lingayat, A.B.; Chandramohan, V.; Raju, V.; Meda, V. A review on indirect type solar dryers for agricultural crops—Dryer setup, its performance, energy storage and important highlights. *Appl. Energy* **2019**, *258*, 114005. [[CrossRef](#)]
27. Boughali, S.; Benmoussa, H.; Bouchekima, B.; Mennouche, D.; Bouguettaia, H.; Bechki, D. Crop drying by indirect active hybrid solar—Electrical dryer in the eastern Algerian Septentrional Sahara. *Sol. Energy* **2009**, *83*, 2223–2232. [[CrossRef](#)]
28. Tun, M.M.; Juchelková, D. Drying methods for municipal solid waste quality improvement in the developed and developing countries: A review. *Environ. Eng. Res.* **2019**, *24*, 529–542. [[CrossRef](#)]

29. de León, J.A.S.; Alanís-López, L. A Mathematical Model for the Prediction of the Scale Layer Formation on ASTM A510/A853 Cold-Drawn Hypoeutectoid Steel Wire After Batch Annealing. *Oxid. Met.* **2022**, *97*, 539–558. [CrossRef]
30. Tang, J.; Zhuang, J.; Aljerf, L.; Xia, H.; Wang, T.; Gao, B. Numerical simulation modelling on whole municipal solid waste incineration process by coupling multiple software for the analysis of grate speed and air volume ratio. *Process. Saf. Environ. Prot.* **2023**, *176*, 506–527. [CrossRef]
31. Jeong, J.-W.; Cao, J.; Aydin, D.; Bottarelli, M.; Jimenez-Bescos, C.; Ghaderi, M.; Reddick, C.; Sorin, M. A Systematic Heat Recovery Approach for Designing Integrated Heating, Cooling, and Ventilation Systems for Greenhouses. *Energies* **2023**, *16*, 5493. [CrossRef]
32. Hwang, J.-K.; Yi, I.-C.; Son, I.-H.; Yoo, J.-Y.; Kim, B.; Zargarán, A.; Kim, N.J. Microstructural evolution and deformation behavior of twinning-induced plasticity (TWIP) steel during wire drawing. *Mater. Sci. Eng. A* **2015**, *644*, 41–52. [CrossRef]
33. Kacprzak, K.; Fijałkowski, K.; Grobelak, A.; Rosikón, K.; Rorat, A. *Escherichia coli* and *Salmonella* spp. Early Diagnosis and Seasonal Monitoring in the Sewage Treatment Process by EMA-qPCR Method. *Polish J. Microbiol.* **2014**, *64*, 143–148.
34. Udayanga, W.C.; Veksha, A.; Giannis, A.; Lisak, G.; Lim, T.-T. Effects of sewage sludge organic and inorganic constituents on the properties of pyrolysis products. *Energy Convers. Manag.* **2019**, *196*, 1410–1419. [CrossRef]
35. Naicker, J.E.; Govinden, R.; Lekha, P.; Sithole, B. Transformation of pulp and paper mill sludge (PPMS) into a glucose-rich hydrolysate using green chemistry: Assessing pretreatment methods for enhanced hydrolysis. *J. Environ. Manag.* **2020**, *270*, 110914. [CrossRef]
36. Brazil Steel Institute. *Statistical Yearbook*; Brazil Steel Institute: Rio de Janeiro, Brazil, 2020; ISSN 1806-3195.
37. A Siderurgia em Números 2022. Available online: https://acobrasil.org.br/site/wp-content/uploads/2022/05/AcoBrasil_Mini_anuario_2022.pdf (accessed on 25 February 2023).
38. Fonseca, D.C. Metodologia para Reciclagem de Resíduos Sólidos Industriais. Ph.D. Thesis, Min. Eng.—Fed. Univ. Minas Gerais, Belo Horizonte, Brazil, 2000.
39. Bhagwat, A.; Ojha, C.S.P. Distributed mathematical model for simulating temperature profile in landfill. *Waste Manag.* **2023**, *167*, 64–73. [CrossRef]
40. ABNT. ABNT NBR 10004: Resíduos Sólidos—Classificação (Solid waste classification). *Assoc. Bras. Normas Técnicas* **2004**, *18*, 71.
41. Leon, M.A.; Kumar, S.; Bhattacharya, S. A comprehensive procedure for performance evaluation of solar food dryers. *Renew. Sustain. Energy Rev.* **2002**, *6*, 367–393. [CrossRef]
42. Duffie, J.A.; Beckman, W.A. *Solar Engineering of Thermal Processes*; John Wiley & Sons: New York, NY, USA, 2013.
43. Versteeg, H.K.; Malalasekera, W.; Prentice, P.; Harlow, H. *An Introduction to Computational Fluid Dynamics*, 2nd ed.; Pearson Education: London, UK, 2007.
44. Guo, C.; Zhou, C.; Liu, X.; Liu, Q. Dehydration kinetics of antibiotic fermentation residues by dehydration agents at room temperature. *Environ. Prog. Sustain. Energy* **2021**, *40*, e13596. [CrossRef]
45. Xu, J.; Li, T.; Yan, T.; Chao, J.; Wang, R. Dehydration kinetics and thermodynamics of magnesium chloride hexahydrate for thermal energy storage. *Sol. Energy Mater. Sol. Cells* **2020**, *219*, 110819. [CrossRef]
46. Höfflin, D.; Sauer, C.; Schiffler, A.; Hartmann, J. Process Monitoring Using Synchronized Path Infrared Thermography in PBF-LB/M. *Sensors* **2022**, *22*, 5943. [CrossRef] [PubMed]
47. Li, X.; Qiu, H.; Wang, Z.; Li, J.; Yuan, G.; Guo, X.; Jin, L. Numerical Investigation of a Solar-Heating System with Solar-Tower Receiver and Seasonal Storage in Northern China: Dynamic Performance Assessment and Operation Strategy Analysis. *Energies* **2023**, *16*, 5505. [CrossRef]
48. Manno, D.; Cipriani, G.; Ciulla, G.; Di Dio, V.; Guarino, S.; Brano, V.L. Deep learning strategies for automatic fault diagnosis in photovoltaic systems by thermographic images. *Energy Convers. Manag.* **2021**, *241*, 114315. [CrossRef]
49. Rebolledo-Lozano, G.A.; Restrepo-Tarquino, I. Potential reuse of industrial sludge in the production of ceramic floor mortar INGENIERÍA AMBIENTAL. *Ing. Compet.* **2020**, *1*, 8023. [CrossRef]
50. Chen, H.-J.; Chen, P.-C.; Peng, C.-F.; Huang, C.-W. Production of Synthetic Lightweight Aggregates from Industrial Sludge. *Materials* **2022**, *15*, 4097. [CrossRef]
51. Duffie, J.A.; Beckman, W.A. *Solar Engineering of Thermal Processes*, 3rd ed.; Wiley: New York, NY, USA, 2006.

Disclaimer/Publisher's Note: The statements, opinions and data contained in all publications are solely those of the individual author(s) and contributor(s) and not of MDPI and/or the editor(s). MDPI and/or the editor(s) disclaim responsibility for any injury to people or property resulting from any ideas, methods, instructions or products referred to in the content.